Fiber-optic bend sensor using LP_{21} mode operation

Yuqiang Fan,[1] George Wu,[1] Wanting Wei,[1] Yufeng Yuan,[1] Feng Lin,[2] and X. Wu[1,*]

[1] *Department of Optical Engineering, Zhejiang University, Hangzhou, Zhejiang 310027, China*
[2] *School of Computer Engineering, Nanyang Technological University, 637553, Singapore*
**xingkunwu@zju.edu.cn*

Abstract: A novel fiber-optic bending sensor based upon the propagation of LP_{21} mode is demonstrated. The sensor, comprised of an S-bend fiber on an elastic film, measures LP_{21} mode specklegram rotation, which increments linearly with bending angle by the stress-optic effect. The sensor is capable of experimentally achieving a sensitivity as high as 4.13 rad/m^{-1}. The theoretical analysis of the sensor, which is a combination of fiber coupled-mode theory and elastic-optic theory, validates the accuracy of the sensor. The sensor is also shown to be temperature-immune, and can detect both bending direction and bending angle with a large dynamic range. Furthermore, the sensor implementation incorporates inexpensive single-mode fiber at 650 nm for few-mode operation, enabling low-loss transmission and compatibility with existing interfaces.

OCIS codes: (060.2350) Fiber optics imaging; (060.2370) Fiber optics sensors ;(110.6150) Speckle imaging.

References and links

1. B. Culshaw and A. Kersey, "Fiber-optic sensing: a historical perspective," J. Lightwave Technol. **26**(9), 1064–1078 (2008).
2. G. M. H. Flockhart, W. N. MacPherson, J. S. Barton, J. D. C. Jones, L. Zhang, and I. Bennion, "Two-axis bend measurement with Bragg gratings in multicore optical fiber," Opt. Lett. **28**(6), 387–389 (2003).
3. C. Y. Lin, L. A. Wang, and G. W. Chem, "Corrugated long-period fiber gratings as strain, torsion, and bending sensors," J. Lightwave Technol. **19**(8), 1159–1168 (2001).
4. L.-Y. Shao, A. Laronche, M. Smietana, P. Mikulic, W. J. Bock, and J. Albert, "Highly sensitive bend sensor with hybrid long-period and tilted fiber Bragg grating," Opt. Commun. **283**(13), 2690–2694 (2010).
5. A. Harhira, J. Lapointe, and Raman Kashyap, "A simple bend sensor using a twin core fiber Mach-Zehnder interferometer," in Proceedings of Latin America Optics and Photonics Conference, Brazil, Paper Tuf3 (2010).
6. L. Yuan, "Recent progress of multi-core fiber based integrated interferometers," Proc. SPIE 7508, 2009 International Conference on Optical Instruments and Technology, 750802; doi:10.1117/12.837912.
7. M. G. Xu, J.-L. Archambault, L. Reekie, and J. P. Dakin, "Thermally-compensated Bending gauge using surface-mounted fibre gratings," Int. J. Optoelectron. **9**(3), 281–283 (1994).
8. Y.-S. Yu, Z.-Y. Zhao, Z.-C. Zhuo, W. Zheng, Y. Qian, and Y.-S. Zhang, "Bend sensor using an embedded etched fiber Bragg grating," Microw. Opt. Technol. Lett. **43**(5), 414–417 (2004).
9. Y. Yuan, G. Wu, X. Li, Y. Fan, and X. Wu, "Effects of twisting and bending on LP_{21} mode propagation in optical fiber," Opt. Lett. **36**(21), 4248–4250 (2011).
10. R. Ulrich and A. Simon, "Polarization optics of twisted single-mode fibers," Appl. Opt. **18**(13), 2241–2251 (1979).
11. N. F. Borrelli and R. A. Miller, "Determination of the Individual Strain-Optic Coefficients of Glass by an Ultrasonic Technique," Appl. Opt. **7**(5), 745–750 (1968).
12. H. J. El-Khozondar, M. S. Müller, T. C. Buck, R. J. El-Khozondar, and A. W. Koch, "Experimental Investigation on Polarization Rotation in Twisted Optical Fiber Using Laboratory Coordinate System," Fiber Integr. Opt. **29**(1), 1–9 (2009).
13. A. M. Smith, "Birefringence induced by bends and twists in single-mode optical fiber," Appl. Opt. **19**(15), 2606–2611 (1980).
14. A. Gray, *The Helix and Its Generalizations,* 2nd ed. (CRC Press, 1997), pp. 198–200.
15. A. J. Barlow and D. N. Payne, "The Stress-Optic Effect in optical fibers," IEEE J. Quantum Electron. **19**(5), 834–839 (1983).

#176543 - $15.00 USD Received 20 Sep 2012; revised 24 Oct 2012; accepted 24 Oct 2012; published 5 Nov 2012

1. Introduction

Measurement of fiber bending using intrinsic fiber sensors presents an attractive alternative to extrinsic electronic bend sensors, with the desirable properties of electromagnetic interference immunity, corrosion resistance, and compact size [1]. Three major classes of fiber-optic bend sensors have been investigated: (1) multi-core bend sensors utilizing multiple beam interference, and (2) fiber Bragg grating (FBG) sensors based on strain-induced spectroscopic properties [2], and (3) long-period fiber grating (LPG) bend sensors, which can be used alone or combined with FBG sensors for precision [3, 4]. Multi-core fibers are capable of measuring bending angle and direction by analyzing interference patterns generated by multiple beams from a segment of two- or four-core fiber bundle due to strain-induced change in refractive index and geometrical factor, and the bend is sensed simply through analyzing interference pattern recorded by a CCD [5, 6]. FBG bend sensors have been proposed utilizing two Bragg wavelengths, via the detection of increased bandwidth broadening with increased curvature using a chirp in the grating period [7, 8]. LPG bend sensors instead incorporate detection for bend-induced wavelength shift, or changes in the attenuation bands. However, though some athermalized designs have been proposed, the output of most existing fiber-grating-based bend sensors are still temperature-dependent, as well as dependent on sophisticated wavelength-resolving peripherals. To improve on existing designs and reduce complexity, thermal effects, and dedicated extrinsic peripherals, we propose an intrinsic fiber sensor a bend sensor of a common single mode fiber operated in few-modes, such as LP_{11} or LP_{21}, intrinsically traveling with two or four lobes in its power distribution.

A fiber-based bending sensor is demonstrated in this paper composed of a small S-shaped fiber segment, operated in LP_{21} mode. The distinctive propagation properties of LP_{21} mode have been reported previously, with an intensity distribution (specklegram) which only rotates linearly with fiber twist angle, but independent of bending angle [9]. When the sensor segment is bent, the S-shaped curve twists, altering the specklegram in rotation angle and direction, which are subsequently translated to bending angle and plane at a given segment respectively. This provides an improvement over existing bend sensors, as LP_{21} mode specklegram propagation is temperature-insensitive as well as extrinsic-bending-immune: the fiber bending of any non-S-shaped segment does not alter the resulting specklegram in rotation or in deformation. The sensor suffers no optical leakage and requires no other mounted peripherals, minimizing power loss. These features make it possible for the LP_{21} bend sensor to be scalable and combined in distributed arrays for complex class of applications, such as multi-jointed, multi-axis independently rotating robotic mechanism in temperature-variable environments. By observing multiple such optical fiber sensors along a fiber ribbon to acquire individual bending values at multiple points, the spatial coordinates of any point along a multiple-jointed system can be obtained. Specific applications for this type of sensor can include posture measurement, minimally invasive surgical devices, virtual reality, and robotic control.

2. Theory

Previously, the obtained propagation properties of pure LP_{21} mode both experimentally and theoretically have been published [9]. The LP_{21} specklegram remains unchanged under fiber bending and or in kilometer-long fiber; under fiber twisting, the specklegram rotates by an angle linearly proportional to the twist angle due to both opto-elastic and geometrical effects.

LP_{21} mode is a low-order propagation mode (few-mode) propagating through a cylindrical waveguide, and has a quadruple-lobed specklegram distributed symmetrically around the center. LP_{21} mode can be either one of two combinations of HE_{31} and EH_{11}: $LP_{21} = HE_{31} \pm EH_{11}$, derived from the Maxwell's equations. $HE_{31} + EH_{11}$, e.g., takes the form:

#176543 - $15.00 USD Received 20 Sep 2012; revised 24 Oct 2012; accepted 24 Oct 2012; published 5 Nov 2012

$$
\begin{aligned}
&E_{xLP_{21}} = E_{xHE_{31}} + E_{xEH_{11}} = 0 \\
&E_{yLP_{21}} = E_{yHE_{31}} + E_{yEH_{11}} = -\frac{2i\,\beta a}{u^2 r}\left[-2aJ_1(\frac{ur}{a}) + urJ_0(\frac{ur}{a})\right]\sin(2\varphi+\theta_0) \qquad (1) \\
&E_{zLP_{21}} = E_{zHE_{31}} + E_{zEH_{11}} = J_3(\frac{ur}{a})\cos(3\varphi+\theta_0) + J_1(\frac{ur}{a})\cos(\varphi+\theta_0)
\end{aligned}
$$

Where β is the propagation constant in the z direction, *a* is the fiber core diameter, J is the Bessel function, and u is the propagation constant for both x and y directions. Further, r, φ, θ_0 are the radial distance, phase angle, and initial phase angle between 0° and 90° respectively.

It can be seen that the longitudinal component is much smaller than the transverse component; therefore, the LP_{21} mode is linearly polarized along y-axis. According to Eq. (1), LP_{21} mode has two orthogonal states: an odd state at $\theta = 0°$, and an even state at $\theta = 90°$.

Generally, when a fiber is being twisted, its specklegram will be affected simultaneously by both geometric and opto-elastic effects. The geometric effect rotates the specklegram in the same direction as the applied external rotation of the fiber. The opto-elastic effect applies an additional effect to the specklegram through a change in the mode field by refractive index perturbation, which can be modeled by coupling wave equations of the odd and even states:

$$
\begin{aligned}
dc_1/dz &= K_{odd\text{-}odd}c_1 + K_{odd\text{-}even}c_2, c_1(0) = 1, \\
dc_2/dz &= K_{even\text{-}odd}c_1 + K_{even\text{-}even}c_2, c_2(0) = m.
\end{aligned} \qquad (2)
$$

Where the coupling coefficients $K_{\alpha\beta}$ for all LP_{21} odd and even states can be defined as

$$
K_{\alpha\beta} = \frac{\omega\varepsilon_0}{4iP_\beta}\iint_D \sum_{i,j=1\text{-}3}\left(E^{\alpha*}_i \Delta n^2_{ij} E^{\beta}_j\right)dxdy\,, \qquad (3)
$$

With *α, β* = 1-4, E^{α}_i represents the i_{th} component of the α_{th} mode electric field (with *α, β* = 1-4 denoting the states of $LP_{21}{}^{+}$ odd, $LP_{21}{}^{-}$ odd, $LP_{21}{}^{+}$ even and $LP_{21}{}^{-}$ even, respectively). P_β is the mode power of the β_{th} mode, and symmetric Δn_{ij} can be modeled by $\Delta n_{42} = -n_4 p_{44}\xi x$, $\Delta n_{52} = n_4 p_{44}\xi y$, where Δn_{ij} is the variation of refractive index, p_{44} is the elastic-optic tensor coefficient, and ξ is the twist rate defined by the twist angle per unit length [10]. A computer-based symbolic calculation yields $K_{ij} = 0$ for the LP_{21} mode: $K_{ij} = 0$ for $(i,j) \neq (1,3), (3,1), (2,4)$ or $(4,2)$, and $K_{13} = -K_{31} = \eta\xi p_{44}(2u^2J_0^2(u) + 4uJ_0(u)J_1(u) + (3u^2 - 16)\,J_1^2(u))$, $K_{24} = -K_{42} = \eta\xi p_{44}(2u^2J_0^2(u) - 4uJ_0(u)J_1(u) + u^2J_1^2(u))$, where $\eta = -\omega^2\varepsilon_0\mu_0 n^4/2\beta^2(u^2J_0^2(u) + (u^2 - 4)J_1^2(u))$ [9].

The field intensity distribution of the specklegram was obtained by solving coupling wave equations. For a twist angle of $\Delta\alpha = \xi z$, the specklegram is rotated by an angle of $\Delta\varphi = n_2 p_{44}\Delta\alpha/2$. Accounting for the mechanical properties of fused silica fiber [11, 12] n = 1.458 and $p_{44} = 0.5(p_{11}-p_{12}) = -0.0780$, we arrive at $\Delta\varphi/\Delta\alpha = n_2 p_{44}/2 = -0.0829$ and thus the calculated net specklegram rotation due to combined geometric and opto-elastic effect of $\Delta\varphi/\Delta\alpha = 1 + n_2 p_{44}/2 = 1 - 0.0829 = 0.9171$.

Similarly, a pure fiber bending introduces a refractive index perturbation Δn_{ij} to the fiber [13]: $\Delta n_{12} = \Delta n_{22} = -n_2\,(n_2 q_1 x/R) + n_2(n_2 q_1 x/R)^2$, $\Delta n_{32} = -n_2(n_2 q_2 x/R) + n_2(n_2 q_3 x/R)^2$, $\Delta n_{42} = \Delta n_{52} = \Delta n_{62} = 0$. Using Δn_{ij} in the aforementioned K_{ij} expression, we obtain: $K_{odd\text{-}even} = K_{even\text{-}odd} = 0$, and

$$
K_{\pi-\pi} = \frac{\omega\varepsilon_0}{4iP_j}\iint_D\left(E_y^{*\pi}\Delta n_2^2 E_y^{\pi} + E_z^{*\pi}\Delta n_3^2 E_z^{\pi}\right)dxdy\,, \qquad (4)
$$

Where $\Delta n_{11} = \Delta n_1, \Delta n_{22} = \Delta n_2, \Delta n_{33} = \Delta n_3, \Delta n_{23(\text{or } 32)} = \Delta n_4, \Delta n_{13(\text{or } 31)} = \Delta n_5, \Delta n_{12(\text{or } 21)} = \Delta n_6$, π = parity = odd or even, and j = 1, 2 for odd and even, respectively. Under fiber mode theory, the

#176543 - $15.00 USD Received 20 Sep 2012; revised 24 Oct 2012; accepted 24 Oct 2012; published 5 Nov 2012

longitudinal component of LP_{21} mode is much smaller than its lateral components; therefore the above expression can be simplified without the longitudinal component, yielding $K_{odd\text{-}odd} = K_{even\text{-}even} = iW$, where $W = a^2n^2q_1^2\eta[(12u + u^3)J_0^2(\mathrm{u}) + (2u^2 - 24)J_0(\mathrm{u})J_1(\mathrm{u}) + (u^3 - 2u)J_1^2(u)]/6uR^2$. As W is real, both $K_{odd\text{-}odd}$ and $K_{even\text{-}even}$ are thus imaginary and $K_{odd\text{-}odd} = K_{even\text{-}even}$. It follows that the odd and even modes have self-coupling, but no inter-coupling, and carries the opposite effect to the relationships found in fiber twisting. The wave equation is thereby modeled by the following: $\mathrm{d}c_1/\mathrm{d}z = K_{\text{odd-odd}}c_1$, $c_1(0) = 1$, $\mathrm{d}c_2/\mathrm{d}z = K_{\text{even-even}}c_2$, $c_2(0) = m$, which gives solution $c_1 = exp(K_{odd\text{-}odd}\, z)$, $c_2 = mexp(K_{even\text{-}even}z)$, and the post-bending electric field $E'_y = c_1E_{1y} + c_2E_{2y} = e^{iWz}E_y$. This signifies that light intensity distribution remains unchanged during bending: $I' = (\mathbf{E}')^*\cdot(\mathbf{E}') = I$. The bending instead introduces a phase to the two separate modes. In the discussion above, small couplings is neglected between LP_{21} and LP_{1x} or LP_{3x} caused by a tilted index profile in relation to a fiber bending, as experimental observation shows that the LP_{21} mode remains stable for a bending radius of as small as 4 mm.

Therefore, under pure fiber twisting, the LP_{21} mode specklegram rotates around its geometric center without changing its radial field distribution; in the case of few-mode operation in a G.652 fiber the specklegram rotates 91.73% of the fiber twist angle. Under pure fiber bending, the specklegram of LP_{21} remains unchanged, exhibiting neither rotation nor deformation. The above theoretical analysis was confirmed experimentally up to a fiber twist angle of 1200° with high accuracy. Based on these propagation features of LP_{21} mode, a fiber bend sensor was designed that contains an S-shaped segment as a sensing element, which twists in response to external bending of the sensor. Because nearly no optical loss is introduced by the sensing mechanism, the bending signal can transfer a long distance or superimposed upon other bends along the path.

3. Experiment and result

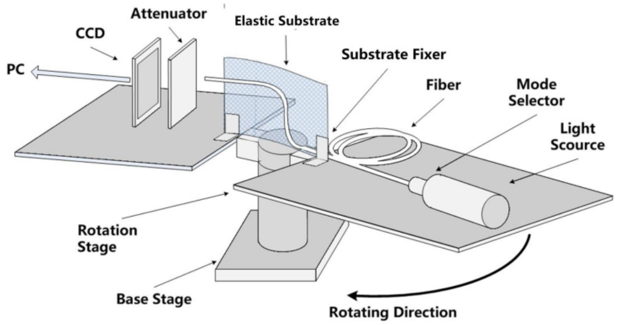

Fig. 1. Schematic of experimental setup

Figure 1 displays a schematic of the experimental setup. A laser diode (658 nm ML120G21 Mitsubishi) and a mode selector were affixed onto a base plate mounted on a rotary stage. A standard G.652 fiber (ITU-T G.652 SMF, Sumitomo Electric), a multimode fiber for 650 nm operation, was used in the fiber bend sensor test. One end of the fiber was affixed to a stationary fiber holder, and the other to a fiber holder mounted on a rotary stage. An S-shaped segment between the two ends formed the sensor body, and was held in position by an elastic substrate. A computer-interfaced CCD camera recorded the output specklegram. Extreme care was exercised to ensure the generation of a pure LP_{21} mode in the duration of the experiment. The mode selector was fabricated from two ceramic fiber ferrules, and a micro-lens mounted on a two-axis rotary stage, which was used to focus the beam (N.A.≈0.05-0.1) into the input end of fiber using a skew ray with its incidence angles (both yaw and pitch) of < 5° with respect to central axis of symmetry of the receiving fiber. This was necessary in order to effectively excite the LP_{21} mode. By minutely adjusting both angles, the modes are gradually

Received 20 Sep 2012; revised 24 Oct 2012; accepted 24 Oct 2012; published 5 Nov 2012

observed to transform from single-lobed, to double-lobed, then finally to quadruple-lobed configurations. Mode configuration was observed to be very stable, capable of maintaining its intensity distribution for over 3-4 hours with a stable mechanical structure; the quadruple-lobe distribution of LP_{21} remains unchanged even after passing through a 2 km-long fiber reel.

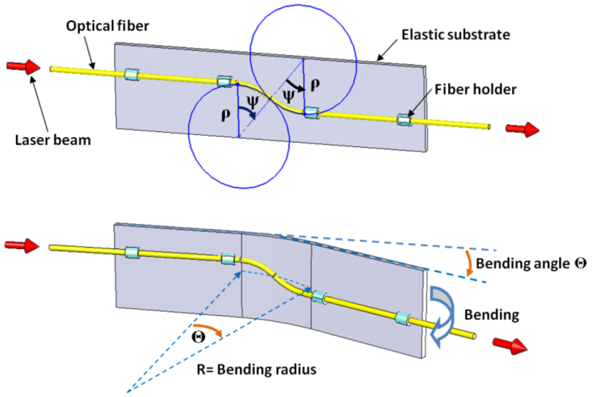

Fig. 2. Structure of the fiber bend sensor

The structure of our sensing fiber, mounted on an elastic, springy substrate (100 μm stainless steel sheet), is shown in Fig. 2. We used a curved fiber segment which consisted of two opposing curvatures with matched circular radii r and central angle α. The radii of curvature met tangentially, with straight parallel leads exiting on both ends of the curvature. The sensing fiber is protected by a polyethylene sleeve (I.D. 0.3mm, O.D. 0.8mm) affixed onto the steel sheet by epoxy, and then retained by four fiber holders, thereby ensuring the fiber segment twists smoothly during substrate bending. Experimental bending radius calibration was accomplished by bending the substrate around machined aluminum cylinders of differing diameters. Bending the sensor substrate leads to both fiber twisting and bending due to helical torsion; however, only the fiber twisting contributes to the rotation of the output specklegram. The sensor is capable of measuring either inward or outward bending, the experimental data given below is for inward bending.

The fiber twist angle can be obtained using helix formulas. When the sensor substrate is bent by an angle of with a circular bending radius R, Θ is related to the above fiber segment dimensions: $\Theta = 2\rho\sin\psi/R$. For a circular helix, torsion τ (twist angle per unit length) can be expressed as $\tau = c/(c^2 + R^2) = \sin\psi\cos\psi/R$, where R is the radius of the helix, ψ is the helix angle and 2πc is a constant giving the vertical separation of the helical loops [14]. By treating the curved fiber as a series of helices with helix angles spanning from 0 to ψ, total fiber twist angle Ω can be calculated by integration of τ over the arc length:

$$\Omega = 2\int_0^{\psi} \tau ds = 2\int_0^{\psi} \frac{\rho}{R}\sin\psi'\cos\psi' d\psi' = \frac{\rho}{R}\sin^2\psi = \frac{1}{2}\Theta\sin\psi, \tag{5}$$

The fiber twisting angle Ω is therefore linearly proportional to the bending angle Θ. For any given ψ, a greater set value of fiber radius ψ would produce a stronger twisting effect, altering the sensitivity of the sensor.

Taking into account the various factors of sensitivity, sensor size and power loss caused by a small fiber bending radius, four sets of parameters were chosen for experimentation: 1) ψ = 10°, ρ = 25 mm; 2) ψ = 20°, ρ = 20 mm; 3) ψ = 30°, ρ = 15 mm; and 4) ψ = 40°, ρ = 10 mm. The sensor has a substrate area of less than 15 × 10 mm^2, and LP_{21} mode power loss is under 5%.

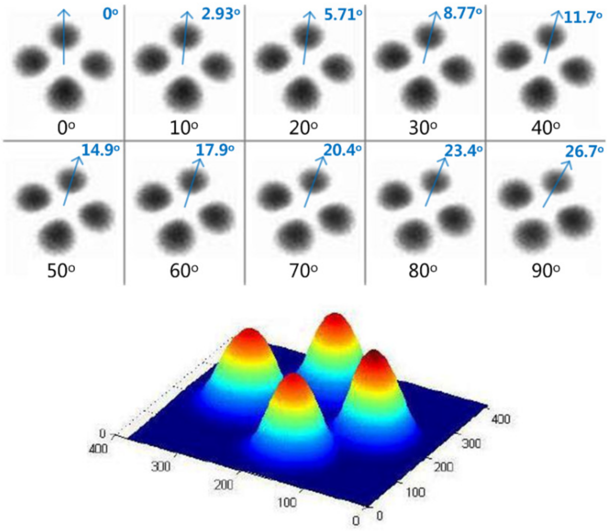

Fig. 3. (Upper) Measured specklegram as bending angle varied from 0°to 90° ($\alpha = 40°$, r = 10 mm), (Lower) Typical intensity distribution of LP21 after processing of Matlab algorithm

Figure 3 (upper) shows selected experimental image data demonstrating the rotation of the LP_{21} specklegram as a function of bending angle of the sensor from 0° to 90° with a step size of 10°. It can be seen that the specklegrams maintain the quadruple-lobe configuration of the original LP_{21} mode with a minimal observed deformation. The value marked near the arrows denote the rotational angles of the specklegram, obtained by a least-squares regression MATLAB® algorithm that fits the intensity peaks of the four lobes in pre- and post-twisting. Specifically, the algorithm for determining the lobe centers first 1) averages the light intensity at every point/pixel p(x,y) within a circle surrounding p(x,y), where the radius of the circle is 15% of the lobe width, then 2) the lobe center is determined by locating the peak of fitted contour. Typical intensity distribution after this processing is shown in Fig. 3 (lower).

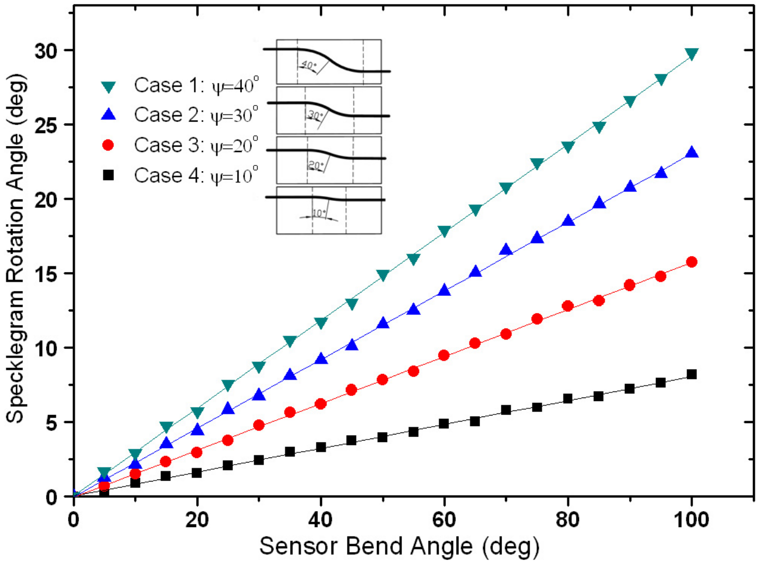

Fig. 4. Specklegram rotation angle versus sensor bending angle at different fiber arc angle ψ.

#176543 - $15.00 USD Received 20 Sep 2012; revised 24 Oct 2012; accepted 24 Oct 2012; published 5 Nov 2012

Figure 4 shows the rotation of the LP_{21} specklegram as a function of the sensor bend angle. The specklegram rotation was found to be linearly proportional to the fiber twist angle. A linear regression of the experimental measurements for case 1-4 reveals slopes of 0.0822, 0.1562, 0.2307, and 0.2960, which corresponds to actual specklegram rotation of 8.22°, 15.62°, 23.07°, and 29.60° at curvature angle ψ of 10, 20, 30, and 40 degrees respectively with the bending angle of the elastic steel plate set at 100°. The direction of the specklegram rotation corresponds to the fiber torsion direction.

According to Eq. (5), for $\Theta = 100°$, and $\psi = 10°$, 20°, 30°, and 40°, the expected fiber twist angles should be 8.67°, 17.10°, 25.00°, and 32.13° respectively. Hence ratios of the measured specklegram rotation angle to the expected fiber twisting angles are 0.9272, 0.9138, 0.9232, and 0.9214 respectively, with a mean ratio of 0.9214. This experimentally verified rotation-twisting ratio deviates from the theoretical value of 0.9173 by less than 0.5%. For the configuration of two circular arcs, sensitivity of the LP_{21} fiber bend sensor depends on the central angle ψ and arc length of curved segment $L = 2\psi\rho$. When $\psi = 40°$ and $L = 14$ mm, the sensitivity reaches 4.13 rad/m^{-1} (in the unit of specklegram rotation angle per bending curvature change). The best estimate of sensor resolution is $10^{-5}m^{-1}$, though exact determination of the resolution is influenced by expected experimental errors of 0.02°, mainly due to the accuracy of peak recognition in the MATLAB algorithm. Compared with existing FBG bend sensors and long-period fiber grating sensors with a resolution ranging from 10^{-3} to 10^{-4} m^{-1} [4], the LP_{21} fiber solution offers both improved sensitivity and resolution.

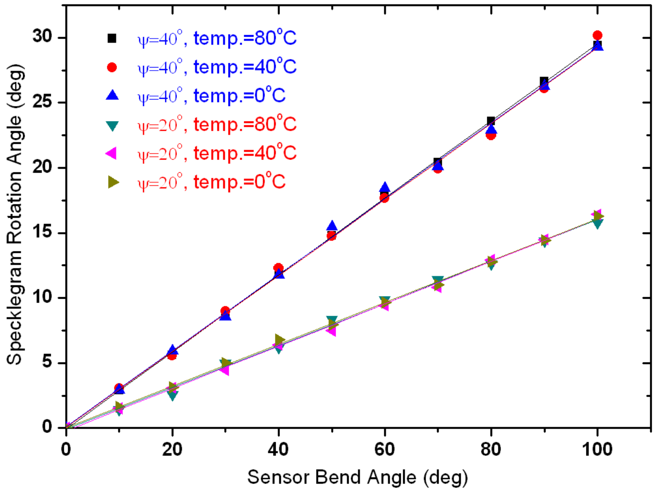

Fig. 5. Specklegram rotation angle versus temperature

The fiber bend sensor was further tested in a temperature-variable water bath in order to determine the effects of temperature on sensor performance. The temperature of the water bath is controlled precisely to ± 0.1°C. Figure 5 shows the specklegram rotation angle as a function of sensor bending angle for two sensitivity settings of $\alpha = 20°$ and 40°, where water temperature varied from 0°C to 80°C. The resulting fluctuation of rotation angle due to temperature variation is observed to be very small, indicating good temperature stability. Table 1 lists percent errors of response slope caused by temperature variation compared to 20°C. The excellent insensitivity of the sensor to temperature is mainly attributable to the fact that the opto-elastic effect $n_2p_{44}/2$ has a very weak temperature dependence. The variation in stress-optic rotation coefficients as low as 0.7% between 0°C and 80°C has been previously reported [15].

Table 1. Experimental result of bending sensor at different fiber arc angles and errors due to different working temperatures

Fiber arc center angle ψ	Ratio of specklegram rotation angle to fiber twist angle	Percent error relative to theoretical value 0.9173, temperature = 20°C	Error due to temperature change/%		
			0°C	40°C	80°C
10°	0.9272	1.01%	0.34	0.21	0.17
20°	0.9138	0.38%	0.31	0.32	0.24
30°	0.9232	0.64%	0.26	0.45	0.31
40°	0.9214	0.45%	0.39	0.62	0.35

4. Conclusions

A novel fiber-based bend sensor based on the stress-optic rotation of LP_{21} mode with a simple inline S-shaped structure was demonstrated and tested experimentally. A sensitivity of 4.13 rad/m^{-1} was obtained for the fiber bend sensor, along with temperature-variance effects of less than 1% when the sensor is operated in the range of 0°C −80°C. Though an S-shaped double circular arc structure with fixed radii was used in this example, the same principle and analysis are readily applicable to similar sensors, with other curved or zig-zag shapes. Further, this inline bend sensor can be arrayed into a fiber ribbon application, allowing for concurrent bend sensing in multiple spots in a single fiber ribbon as LP_{21} mode is immune to bending in non-torsion areas. This sensor demonstrates improved sensitivity, resolution, and temperature-insensitivity over existing FBG- and LFG-based sensors, and holds wide-ranging significance in applications such as medicine and virtual reality.

Acknowledgments

This work was supported by the National Natural Science Foundation of China (NSFC) under the grant 61178049.